Optical trapping of silver nanoplatelets

E. Messina,[1] M. G. Donato,[1,*] M. Zimbone,[2] R. Saija,[3] M. A. Iatì,[1] L. Calcagno,[2] M. E. Fragalà,[4] G. Compagnini,[4] C. D'Andrea,[1] A. Foti,[1,3] P. G. Gucciardi,[1] and O. M. Maragò[1]

[1]*IPCF-CNR, Istituto per i Processi Chimico-Fisici, I-98158, Messina, Italy*
[2]*Dipartimento di Fisica ed Astronomia, Università di Catania, I-95125 Catania, Italy*
[3]*Dipartimento di Fisica e di Scienze della Terra, Università di Messina, I-98166, Messina, Italy*
[4]*Dipartimento di Scienze Chimiche, Università di Catania, I-95125 Catania, Italy*
[*]*donato@me.cnr.it*

Abstract: Optical trapping of silver nanoplatelets obtained with a simple room temperature chemical synthesis technique is reported. Trap spring constants are measured for platelets with different diameters to investigate the size-scaling behaviour. Experimental data are compared with models of optical forces based on the dipole approximation and on electromagnetic scattering within a T-matrix framework. Finally, we discuss applications of these nanoplatelets for surface-enhanced Raman spectroscopy.

OCIS codes: (350.4855) Optical tweezers or optical manipulation; (170.4520) Optical confinement and manipulation; (160.4236) Nanomaterials; (290.5825) Scattering theory.

References and links

1. S. A. Maier, *Plasmonics: Fundamentals and Applications* (Springer, 2007).
2. C. D'Andrea, J. Bochterle, A. Toma, C. Huck, F. Neubrech, E. Messina, B. Fazio, O. M. Maragò, E. Di Fabrizio, M. Lamy de La Chapelle, P. G. Gucciardi, and A. Pucci, "Optical Nanoantennas for Multiband surface-enhanced infrared and Raman spectroscopy," ACS Nano **7**(4), 3522–3531 (2013).
3. H. A. Atwater and A. Polman, "Plasmonics for improved photovoltaic devices," Nat. Mater. **9**(3), 205–213 (2010).
4. C. H. Chou and F. C. Chen, "Plasmonic nanostructures for light trapping in organic photovoltaic devices," Nanoscale **6**(15), 8444–8458 (2014).
5. A. McLeod, A. Weber-Bargioni, Z. Zhang, S. Dhuey, B. Harteneck, J. B. Neaton, S. Cabrini, and P. J. Schuck, "Nonperturbative Visualization of Nanoscale Plasmonic Field Distributions via Photon Localization Microscopy," Phys. Rev. Lett. **106**(3), 037402 (2011).
6. I. Urries, C. Muñoz, L. Gomez, C. Marquina, V. Sebastian, M. Arruebo, and J. Santamaria, "Magneto-plasmonic nanoparticles as theranostic platforms for magnetic resonance imaging, drug delivery and NIR hyperthermia applications," Nanoscale **6**(15), 9230–9240 (2014).
7. W. Xiong, R. Mazid, L. W. Yap, X. Li, and W. Cheng, "Plasmonic caged gold nanorods for near-infrared light controlled drug delivery," Nanoscale **6**(23), 14388–14393 (2014).
8. X. Huang and M. El-Sayed, "Gold nanoparticles: Optical properties and implementations in cancer diagnosis and photothermal therapy," J. Advert. Res. **1**(1), 13–28 (2010).
9. C. Burda, X. Chen, R. Narayanan, and M. A. El-Sayed, "Chemistry and Properties of Nanocrystals of Different Shapes," Chem. Rev. **105**(4), 1025–1102 (2005).
10. G. Compagnini, E. Messina, O. Puglisi, and V. Nicolosi, "Synthesis of Au/Ag colloidal nano-alloys: exploring the optical properties for an accurate analysis," Appl. Surf. Sci. **254**(4), 1007–1011 (2007).
11. V. Amendola, S. Polizzi, and M. Meneghetti, "Laser ablation synthesis of gold nanoparticles in organic solvents," J. Phys. Chem. B **110**(14), 7232–7237 (2006).
12. V. Amendola, S. Polizzi, and M. Meneghetti, "Free silver nanoparticles synthesized by laser ablation in organic solvents and their easy functionalization," Langmuir **23**(12), 6766–6770 (2007).
13. V. Amendola, O. M. Bakr, and F. Stellacci, "A study of the surface plasmon resonance of silver nanoparticles by the discrete dipole approximation method: effect of shape, size, structure and assembly," Plasmonics **5**(1), 85–97 (2010).
14. F. Moreno, P. Albella, and M. Nieto-Vesperinas, "Analysis of the spectral behavior of localized plasmon resonances in the near- and far-field regimes," Langmuir **29**(22), 6715–6721 (2013).
15. K. L. Kelly, E. Coronado, L. L. Zhao, and G. C. Schatz, "The optical properties of metal nanoparticles: the influence of size, shape, and dielectric environment," J. Phys. Chem. B **107**(3), 668–677 (2003).
16. E. Hao, G. C. Schatz, and J. T. Hupp, "Synthesis and optical properties of anisotropic metal nanoparticles," J. Fluoresc. **14**(4), 331–341 (2004).
17. B. J. Wiley, S. H. Im, Z. Y. Li, J. McLellan, A. Siekkinen, and Y. Xia, "Maneuvering the surface plasmon resonance of silver nanostructures through shape-controlled synthesis," J. Phys. Chem. B **110**(32), 15666–15675 (2006).

#232608 - $15.00 USD Received 19 Jan 2015; revised 17 Feb 2015; accepted 23 Feb 2015; published 30 Mar 2015

18. P. Albella, F. Moreno, J. M. Saiz, and F. González, "Surface inspection by monitoring spectral shifts of localized plasmon resonances," Opt. Express **16**(17), 12872–12879 (2008).
19. J. Z. Zhang and C. Noguez, "Plasmonic optical properties and applications of metal nanostructures," Plasmonics **3**(4), 127–150 (2008).
20. A. Ashkin, J. M. Dziedzic, J. E. Bjorkholm, and S. Chu, "Observation of a single-beam gradient force optical trap for dielectric particles," Opt. Lett. **11**(5), 288–290 (1986).
21. K. Dholakia and T. Čižmár, "Shaping the future of manipulation," Nat. Photonics **5**(6), 335–342 (2011).
22. O. M. Maragò, P. H. Jones, P. G. Gucciardi, G. Volpe, and A. C. Ferrari, "Optical trapping and manipulation of nanostructures," Nat. Nanotechnol. **8**(11), 807–819 (2013).
23. K. Svoboda and S. M. Block, "Optical trapping of metallic Rayleigh particles," Opt. Lett. **19**(13), 930–932 (1994).
24. P. M. Hansen, V. K. Bhatia, N. Harrit, and L. Oddershede, "Expanding the optical trapping range of gold nanoparticles," Nano Lett. **5**(10), 1937–1942 (2005).
25. L. Bosanac, T. Aabo, P. M. Bendix, and L. B. Oddershede, "Efficient optical trapping and visualization of silver nanoparticles," Nano Lett. **8**(5), 1486–1491 (2008).
26. M. Pelton, M. Liu, H. Y. Kim, G. Smith, P. Guyot-Sionnest, and N. F. Scherer, "Optical trapping and alignment of single gold nanorods by using plasmon resonances," Opt. Lett. **31**(13), 2075–2077 (2006).
27. C. Selhuber-Unkel, I. Zins, O. Schubert, C. Sönnichsen, and L. B. Oddershede, "Quantitative optical trapping of single gold nanorods," Nano Lett. **8**(9), 2998–3003 (2008).
28. L. Tong, V. D. Miljković, and M. Käll, "Alignment, Rotation, and Spinning of Single Plasmonic Nanoparticles and Nanowires Using Polarization Dependent Optical Forces," Nano Lett. **10**(1), 268–273 (2010).
29. K. C. Toussaint, Jr., M. Liu, M. Pelton, J. Pesic, M. J. Guffey, P. Guyot-Sionnest, and N. F. Scherer, "Plasmon resonance-based optical trapping of single and multiple Au nanoparticles," Opt. Express **15**(19), 12017–12029 (2007).
30. Z. Yan, M. Pelton, L. Vigderman, E. R. Zubarev, and N. F. Scherer, "Why single-beam optical tweezers trap gold nanowires in three dimensions," ACS Nano **7**(10), 8794–8800 (2013).
31. Z. Yan, J. E. Jureller, J. Sweet, M. J. Guffey, M. Pelton, and N. F. Scherer, "Three-Dimensional Optical Trapping and Manipulation of Single Silver Nanowires," Nano Lett. **12**(10), 5155–5161 (2012).
32. E. Messina, E. Cavallaro, A. Cacciola, R. Saija, F. Borghese, P. Denti, B. Fazio, C. D'Andrea, P. G. Gucciardi, M. A. Iatì, M. Meneghetti, G. Compagnini, V. Amendola, and O. M. Maragò, "Manipulation and Raman Spectroscopy with Optically Trapped Metal Nanoparticles Obtained by Pulsed Laser Ablation in Liquids," J. Phys. Chem. C **115**(12), 5115–5122 (2011).
33. E. Messina, E. Cavallaro, A. Cacciola, M. A. Iatì, P. G. Gucciardi, F. Borghese, P. Denti, R. Saija, G. Compagnini, M. Meneghetti, V. Amendola, and O. M. Maragò, "Plasmon-Enhanced Optical Trapping of Gold Nanoaggregates with Selected Optical Properties," ACS Nano **5**(2), 905–913 (2011).
34. E. Messina, L. D'Urso, E. Fazio, C. Satriano, M. G. Donato, C. D'Andrea, O. M. Maragò, P. G. Gucciardi, G. Compagnini, and F. Neri, "Tuning the structural and optical properties of gold/silver nano-alloys prepared by laser ablation in liquids for optical limiting, ultra-sensitive spectroscopy, and optical trapping," J. Quant. Spectros. Ra. **113**(18), 2490–2498 (2012).
35. F. Svedberg, Z. Li, H. Xu, and M. Käll, "Creating hot nanoparticle pairs for surface-enhanced raman spectroscopy through optical manipulation," Nano Lett. **6**(12), 2639–2641 (2006).
36. D. V. Petrov, "Raman spectroscopyof optically trapped particles," J. Opt. A, Pure Appl. Opt. **9**(8), S139–S156 (2007).
37. O. M. Maragó, F. Bonaccorso, R. Saija, G. Privitera, P. G. Gucciardi, M. A. Iatì, G. Calogero, P. H. Jones, F. Borghese, P. Denti, V. Nicolosi, and A. C. Ferrari, "Brownian Motion of Graphene," ACS Nano **4**(12), 7515–7523 (2010).
38. J. Aizpurua and R. Hillenbrand, "Localized surface plasmons: basics and applications in field-enhanced spectroscopy," in *Plasmonics*, Springer Series in Optical Sciences 167, S. Enoch and N. Bonod (eds.) (Springer-Verlag, 2012).
39. G. Volpe and G. Volpe, "Simulation of a Brownian particle in an optical trap," Am. J. Phys. **81**(3), 224–230 (2013).
40. S. H. Simpson, "Inhomogeneous and anisotropic particles in optical traps: physical behaviour and applications," J. Quant. Spectros. Ra. **146**, 81–99 (2014).
41. F. Borghese, P. Denti, R. Saija, and M. A. Iatì, "Radiation torque on nonspherical particles in the transition matrix formalism," Opt. Express **14**(20), 9508–9521 (2006).
42. S. H. Simpson, D. C. Benito, and S. Hanna, "Polarization-induced torque in optical traps," Phys. Rev. A **76**(4), 043408 (2007).
43. T. A. Nieminen, T. Asavei, V. L. Loke, N. R. Heckenberg, and H. Rubinsztein-Dunlop, "Symmetry and the generation and measurement of optical torque," J. Quant. Spectros. Ra. **110**(14-16), 1472–1482 (2009).
44. G. Volpe and D. Petrov, "Torque Detection using Brownian Fluctuations," Phys. Rev. Lett. **97**(21), 210603 (2006).
45. P. H. Jones, F. Palmisano, F. Bonaccorso, P. G. Gucciardi, G. Calogero, A. C. Ferrari, and O. M. Maragó, "Rotation detection in light-driven nanorotors," ACS Nano **3**(10), 3077–3084 (2009).
46. M. G. Donato, J. Hernandez, A. Mazzulla, C. Provenzano, R. Saija, R. Sayed, S. Vasi, A. Magazzù, P. Pagliusi, R. Bartolino, P. G. Gucciardi, O. M. Maragò, and G. Cipparrone, "Polarization-dependent optomechanics mediated by chiral microresonators," Nat. Commun. **5**, 3656 (2014).
47. B. Carrasco and J. García de la Torre, "Hydrodynamic properties of rigid particles: comparison of different modeling and computational procedures," Biophys. J. **76**(6), 3044–3057 (1999).

#232608 - $15.00 USD Received 19 Jan 2015; revised 17 Feb 2015; accepted 23 Feb 2015; published 30 Mar 2015

48. J. G. de la Torre, G. R. Echenique, and A. Ortega, "Improved calculation of rotational diffusion and intrinsic viscosity of bead models for macromolecules and nanoparticles," J. Phys. Chem. B **111**(5), 955–961 (2007).
49. J. Garcia de la Torre, S. Navarro, M. C. Lopez Martinez, F. G. Diaz, and J. J. Lopez Cascales, "HYDRO: a computer program for the prediction of hydrodynamic properties of macromolecules," Biophys. J. **67**(2), 530–531 (1994).
50. R. Saija, P. Denti, F. Borghese, O. M. Maragò, and M. A. Iatì, "Optical trapping calculations for metal nanoparticles. Comparison with experimental data for Au and Ag spheres," Opt. Express **17**(12), 10231–10241 (2009).
51. F. Borghese, P. Denti, and R. Saija, *Scattering from Model Nonspherical Particles* (Springer-Verlag, 2007).
52. C. F. Bohren and D. R. Huffman, *Absorption and Scattering of Light by Small Particles* (John Wiley & Sons, 1998).
53. L. Novotny and B. Hecht, *Principles of Nano-Optics* (Cambridge University, 2008).
54. T. A. Nieminen, H. Rubinsztein-Dunlop, N. R. Heckenberg, and A. I. Bishop, "Numerical modelling of optical trapping," Comput. Phys. Commun. **142**(1-3), 468–471 (2001).
55. F. Borghese, P. Denti, R. Saija, and M. A. Iatì, "Optical trapping of nonspherical particles in the T-matrix formalism," Opt. Express **15**(19), 11984–11998 (2007).
56. S. H. Simpson and S. Hanna, "Optical trapping of spheroidal particles in Gaussian beams," J. Opt. Soc. Am. A **24**(2), 430–443 (2007).
57. T. A. Nieminen, V. L. Loke, A. B. Stilgoe, N. R. Heckenberg, and H. Rubinsztein-Dunlop, "T-matrix method for modelling optical tweezers," J. Mod. Opt. **58**(5-6), 528–544 (2011).
58. A. A. R. Neves, A. Fontes, L. A. Padilha, E. Rodriguez, C. H. Cruz, L. C. Barbosa, and C. L. Cesar, "Exact partial wave expansion of optical beams with respect to an arbitrary origin," Opt. Lett. **31**(16), 2477–2479 (2006).
59. P. B. Johnson and R. W. Christy, "Optical constants of the noble metals," Phys. Rev. B **6**(12), 4370–4379 (1972).
60. J. Lindhard, "On the properties of a gas of charged particles," Mat.-Fys. Medd.—K. Dan. Vidensk. Selsk. **28**, 8 (1954).
61. A. Pack, M. Hietschold, and R. Wannemacher, "Failure of local Mie theory: optical spectra of colloidal aggregates," Opt. Commun. **194**(4-6), 277–287 (2001).
62. E. C. Le Ru, S. A. Meyer, C. Artur, P. G. J. Etchegoin, J. Grand, P. Lang, and F. Maurel, "Experimental Demonstration of surface selection rules for SERS on flat metallic surfaces," Chem. Commun. (Camb.) **47**(13), 3903–3905 (2011).
63. C. D'Andrea, B. Fazio, P. G. Gucciardi, M. C. Giordano, C. Martella, D. Chiappe, A. Toma, F. Buatier de Mongeot, F. Tantussi, P. Vasanthakumar, F. Fuso, and M. Allegrini, "SERS enhancement and field confinement in nanosensors based on self-organizad gold nanowires produced by Ion-Beam sputtering," J. Phys. Chem. C **118**(16), 8571–8580 (2014).
64. G. Xiao and S. Man, "Surface-enhanced Raman scattering of methylene blue adsorbed on cap-shaped silver nanoparticles," Chem. Phys. Lett. **447**(4–6), 305–309 (2007).

1. Introduction

Particles in the nanometer size range have attracted increasing attention with the growing interest in nanoscience and nanotechnology. Among them, metal nanoparticles are extremely appealing due to their plasmonic properties [1]. In fact, collective motions (plasmons) of electrons may be excited by electromagnetic radiations at resonant wavelengths, depending on the material composition, size and shape of the nanoparticle itself. At resonance, amplified electric fields in the close proximity of the nanoparticles may be used not only to enhance optical response of molecules for sensing and/or spectroscopic investigation (SERS, SEIRS and SEIRA effect) [2], but also for applications in photovoltaics [3,4], in nanoscale microscopy [5], in drug delivery [6,7] and even cancer diagnosis and therapy [8].

For practical applications, it is crucial to prepare metal nanoparticles with the desired shape and size distributions. These include spherical nanoparticles, metal nanorods and nanowires, and bidimensional nanoplatelets. A large number of studies are available on the synthesis of metal nanoparticles in solution by different methods such as chemical reduction [9] and laser ablation in liquid environment [10–12]. In this context, silver nanoparticles are of great interest, because, in the visible range, they have more intense and sharper features than other plasmonic metals such as gold or copper associated with smaller absorption [13, 14]. Thus, they represent an important alternative to gold for enhanced spectroscopies in the visible. Silver spherical nanoparticles have a strong dipolar plasmon band at approximately 400 nm. Moreover, as the plasmon resonance depends on particle size and shape, additional dipolar and quadrupolar plasmonic peaks are observed in large spherical particles or for different non-spherical shapes [13, 15–17]. Dipolar resonances due to the increasing size of

#232608 - $15.00 USD Received 19 Jan 2015; revised 17 Feb 2015; accepted 23 Feb 2015; published 30 Mar 2015

particles typically red-shift with respect to dipolar resonances of small spherical particles. Moreover, dipolar resonances may shift to longer wavelengths also due to the presence of a dielectric substrate [18]. Quadrupolar modes, on the contrary, appear at lower wavelengths than dipolar bands [13,19]. This tunability in the plasmonic response is key to a wide range of applications of plasmonic nanoparticles.

Optical tweezers (OT) [20], a valuable tool for the trapping and manipulation of micro [21] and nano-sized [22] particles, have led to a tremendous progress in physics, chemistry, material science and biology. In OT, a laser beam is tightly focused by a high numerical aperture objective. Optical trapping of particles is possible if attractive forces due to the strong gradient of light intensity at the focal point are stronger than the destabilizing effects of the scattering force, due to light scattering and absorption. The higher polarizability of metal nanoparticles with respect to dieletric particles of the same size leads to increased optical gradient force and stronger optical trapping [23]. However, the increased polarizability may also lead to an increased scattering force near a plasmon resonance. Thus, the challenge in optical trapping of metal nanoparticles is to enhance gradient forces while mantaining acceptably low scattering forces.

Optical trapping of metal nanoparticles have been demonstrated on different Au and Ag nanosystems, such as Au [24] and Ag nanospheres [25], Au [26,27] and Ag nanorods [28], Au bypiramids and Au/Ag core/shell nanorods [29], Au [30] and Ag nanowires [28,31], Au [32,33] and Au/Ag alloyed aggregates [34]. In the case of non-spherical particles, the presence of the plasmon resonances in the visible/NIR part of the spectrum may be exploited to enhance the radiation forces by tuning the trapping laser in their proximity [33]. As OT have been integrated with Raman spectroscopy [32,35–37], it is extremely interesting to explore the SERS capability of trapped metal nanoparticles with a wide tunability of their plasmonic response as they could be used for high-resolution spectroscopy applications.

Here we study the optical trapping of bidimensional Ag nanoplatelets with tunable plasmonic properties. They are obtained by a rapid and simple room-temperature technique with variable diameter (39-110 nm). The optical trapping forces and the shape of the trapping potential are measured and compared with models of optical forces based on the dipole approximation for oblate spheroids and on exact electromagnetic calculations in the T-matrix formalism of optical trapping for flat clusters of spherical nanoparticles. Finally, the use of these nanoplatelets for SERS analysis of molecular species is discussed.

2. Experimental

Silver nanoplatelets are obtained by a chemical method via a three step procedure. First, “Ag seeds” are prepared by dropwise addition of $NaBH_4$ solution (20 mM, 0.5 mL) to an aqueous solution of $AgNO_3$ (59 mM, 0.5 mL) in the presence of trisodium citrate (34 mM, 10 ml) under vigorous stirring. The obtained solution is agitated for 20 minutes and left to settle for almost 24 hours at room temperature. Second, 80 µL of “Ag seeds” solution is added rapidly to 50 µL of hydrated hydrazine (400 mM) and 60 µL of trisodium citrate (400 mM). Thus, the mixed solution is stirred for 30 s, “solution 1”. Third, 60 µL of silver nitrate (590 mM) aqueous solution are added to 6 mL of deionized water, “solution 2”. Finally, solution 2 is added dropwise to the solution 1 during steering and samples are extracted at different times during addition. The transverse nanoplatelets size increases with time. Thus, we prepare four different samples at the following times during addition: sample 1 after 2 min., sample 2 after 4 min., sample 3 after 6 min. and samples 4 after 8 min. After extraction, the obtained final solutions persist stable in time, Fig. 1(a).

The structural and morphological characteristics of the samples are investigated by Scanning Electron Microscopy (SEM). SEM images, shown in Fig. 1(b), are acquired by using a SOPRA 25 ZEISS microscope. Images are acquired at working distance of 5-7 mm, using an electron beam of 19 keV and an IN-LENS detector. Scanning was performed at intermediate/low speed, averaging each line scan 10 times. Images are then analyzed with ImageJ software.

#232608 - $15.00 USD Received 19 Jan 2015; revised 17 Feb 2015; accepted 23 Feb 2015; published 30 Mar 2015

Optical UV–Vis spectroscopy is carried out by a Perkin-Elmer Lambda 35 spectrometer in the wavelength range 400–1100 nm using a 1 cm path cell. The growth process of silver nanoplatelets is monitored by measuring UV-Vis spectra for each sample, as shown in Fig. 1(c).

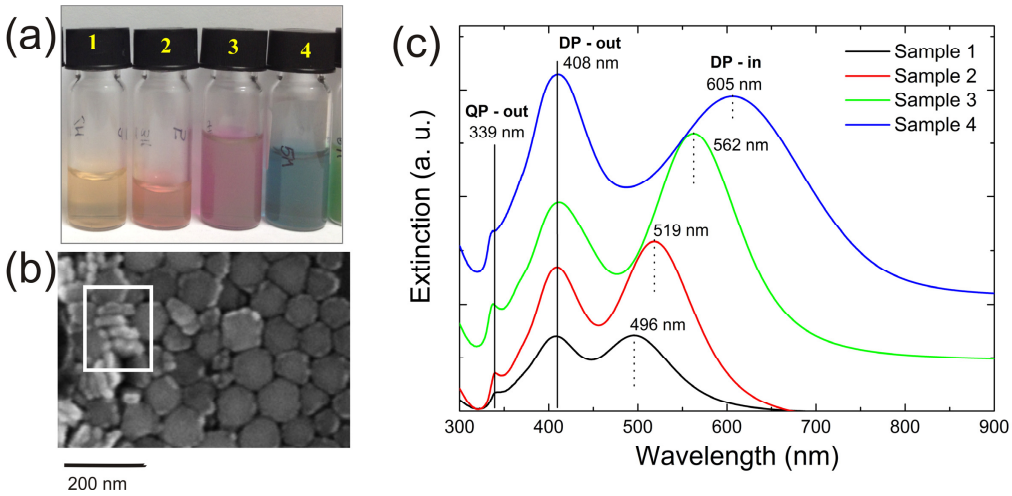

Fig. 1. (a) Image showing the color range of samples studied in this work. (b) Exemplar SEM micrograph of sample 3. The 2D character of the Ag nanoparticles is visible in the inset. (c) Extinction spectra of the different samples in solution. The plasmonic bands centers and their assignations are also indicated: QP – out, out-of-plane quadrupole mode; DP – out, out-of-plane dipole mode; DP – in, in-plane dipole mode. Data are shifted vertically for clarity.

The optical tweezers apparatus is based on an inverted microscope. Optical trapping is accomplished by tightly focusing a laser beam through a high numerical aperture objective (Olympus, Uplan FLN 100X, NA = 1.3). We use a 830 nm, 150 mW laser diode (Sanyo DL-8032-01) as a radiation source. Light power at the sample is approximately 20 mW. A telescope is used to enlarge the beam and overfill the aperture of the objective. Small amounts (about 80 μL) of sample solution are loaded on a slide with a small round chamber. A CCD camera is used to optically inspect and image the samples via the same objective lens that is used for optical trapping. Optical force measurements and calibration of optical tweezers are obtained through interferometry of forward- and unscattered laser light in the back focal plane of the condenser of the microscope. The focal plane of the condenser is projected by a collection lens onto a four-quadrant photodiode (QPD) and the analog outputs from each quadrants are combined to generate signals proportional to the spatial displacements *x,y,z* of the trapped particle (particle tracking).

2. Results and discussion

2.1 Sample characterization

First, in order to have specific information about nanoparticle size and shape, SEM analyses have been performed. To this aim, a drop of each nanoparticle solution was deposited on a Si wafer and left to evaporate in air. The process of evaporation of the solvent induces the formation of very large aggregates; nonetheless, the size and the shape of the obtained nanoparticles can be deduced. As is shown in Fig. 1(b), a nearly circular shape is observed with diameters in the range 39 nm-110 nm (Table 1). As is observed in the inset of Fig. 1(b), a stack of nanoparticles points out their flat shape. The thickness of all samples is approximately 20 nm.

#232608 - $15.00 USD Received 19 Jan 2015; revised 17 Feb 2015; accepted 23 Feb 2015; published 30 Mar 2015

Table 1. Diameter of the nanoplatelets studied in this work. The postion of the in-plane dipolar plasmon resonance band is also indicted.

Sample	Diameter (nm)	Dipolar resonance (nm)
1	39 ± 9	496
2	65 ± 13	519
3	85 ± 8	562
4	110 ± 8	605

The potential applications of the Ag nanoplatelets depend strongly on their optical properties. To investigate them, UV-Vis spectra have been acquired for each sample solution. The spectra of the nanoplatelets, shown in Fig. 1(c), display three extinction bands. The first (339 nm) and the second (408 nm) band do not change in position in all the spectra despite of the different colors of the solutions shown in Fig. 1(a). On the other hand, a red-shift of the third band (from 496 nm to 605 nm) is observed as the sample diameter increases. The occurrence of more than one plasmon resonance is indicative of non-spherical particle shape, as it is connected to an anisotropic polarizability [38]. Considering the two dimensional character of our samples, as shown by SEM investigation, we assign the first and the second band to the quadrupolar (QP - out) and dipolar (DP - out) resonance modes in the out-of-plane direction, respectively. On the contrary, as the third band is strongly dependent on the plate diameter, it is assigned to the in-plane dipolar resonance mode (DP - in). It is worth noting that a UV-Vis systematic study of Ag nanodisks at increasing diameter and fixed thickness has not been reported to date. However, other authors, by means of both Discrete Dipole Approximation (DDA) theory and experimental analysis, gave the same assignations for the first band [16] and third band [16,17], even if the disks they studied were thinner and had smaller diameter. Regarding the second band, it appears quite safe to assign it to the plasmon resonance in the out-of-plane direction, as it remains fixed at the position corresponding to the plasmon resonance for small spherical nanoparticles.

2.2 Optical trapping force measurements

The core of force sensing in optical trapping is the Brownian motion [39]. The dynamics of a trapped brownian spherical particle in water is led by the Langevin equation in the strongly overdamped regime:

$$\frac{d}{dt}x_i(t) = -\omega_i x_i(t) + \xi_i(t) \quad \text{i=x,y,z}, \tag{1}$$

where the relaxation frequencies $\omega_i = \frac{k_i}{\gamma}$ are connected to the trap spring constants k_i and hydrodynamic friction coefficient γ. The term $\xi_i(t)$ describe random uncorrelated fluctuations with zero mean, $\langle \xi_i(t) \rangle = 0$ and temporal correlation related to particle diffusion, namely $\langle \xi(t+\tau)\xi(t) \rangle = 2\frac{k_B T}{\gamma}\delta(\tau)$. As the Ag nanoplatelets trapped in this work are two-dimensional, we have to consider the viscous drag coefficients $\gamma_{\parallel}$ and $\gamma_{\perp}$ in the parallel and perpendicular directions, respectively, to the platelet symmetry axis. Moreover, radiation torque [40–43] orient the platelets with their major axes directed along the field polarization and the beam propagation directions, i.e., the platelets lie in the *xz* plane (see T-matrix calculations below). Thus, within a small angle approximation, for the positional fluctuations we get three decoupled Langevin equations [37]:

$$\frac{d}{dt}x(t) = -\frac{k_x}{\gamma_{\perp}}x(t) + \xi_x(t), \frac{d}{dt}y(t) = -\frac{k_y}{\gamma_{\parallel}}y(t) + \xi_y(t), \frac{d}{dt}z(t) = -\frac{k_z}{\gamma_{\perp}}z(t) + \xi_z(t). \tag{2}$$

#232608 - $15.00 USD Received 19 Jan 2015; revised 17 Feb 2015; accepted 23 Feb 2015; published 30 Mar 2015

To get the spring constants from experimental particle tracking signals, we use a time-domain analysis of their Brownian fluctuations in the trap. This method has been proven useful for the study of forces and torques on trapped micro- and nanoparticles [44–46]. The autocorrelation functions of the particle displacements are:

$$< C_{ii}(\tau) >=< x_i(t)\, x_i(t+\tau) > \tag{3}$$

and from Eqs. (2) we easily obtain that

$$C_{ii}(\tau) = C_{ii}(0)\, e^{-\omega_i \tau}. \tag{4}$$

Thus, fitting the autocorrelations function of the tracking signals obtained by the QPD by a single exponential decay function, we obtain the relaxation frequencies ω_i and, if $\gamma_{\|}$ and $\gamma_{\perp}$ are known, the trap spring constants k_i.

To this aim, we have calculated the translational diffusion coefficients $D_{\|}$ and $D_{\perp}$ following the calculation scheme of Carrasco and Garcia de la Torre [47,48] and the related public software [49]. In particular, we have calculated the diffusion matrix in the orthonormal frame for which it becomes diagonal. The mean translation diffusion coefficients have been computed by taking one-third of the trace of the diffusion matrix tensor. After obtaining $D_{\|}$ and $D_{\perp}$, the friction coefficients $\gamma_{\|}$ and $\gamma_{\perp}$ have been calculated by means of the Einstein-Smoluchowski relation.

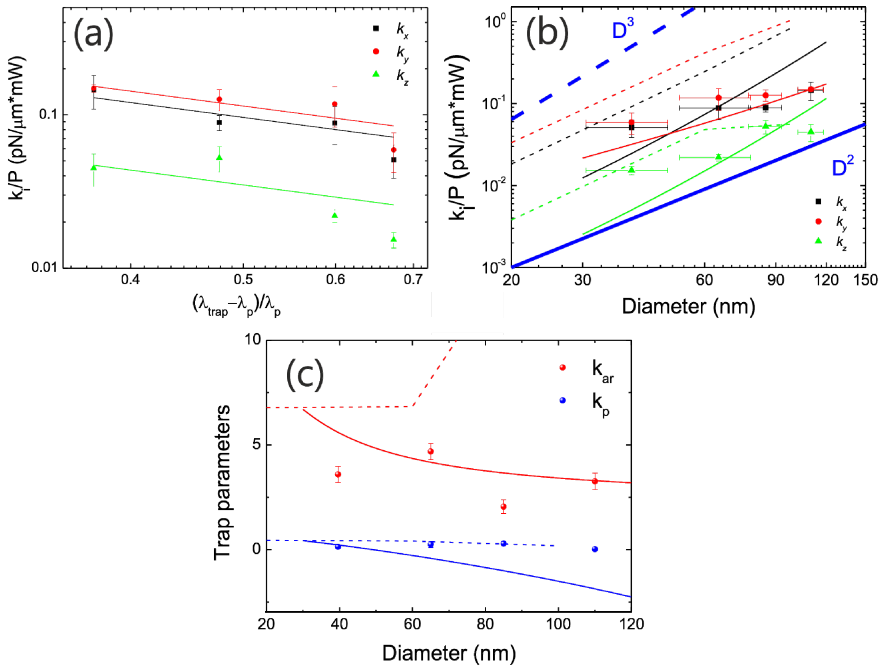

Fig. 2. (a) Trap force constants as a function of the reduced parameter $(\lambda_{trap}-\lambda_p)/\lambda_p$ related to the distance of the trapping wavelength, λ_{trap}, from the in-plane dipole resonance wavelength, λ_p. This is evidence of a frequency scaling of the optical trapping force. Solid lines are a fit to the data with a 1/x scaling. (b) Trap force constants as a function of the platelet diameter (data points). Lines are spring constants obtained in the dipole approximation for an oblate spheroid (solid lines) and by T-matrix calculations on flat clusters of spheres (dashed lines). The thick blue lines are a guide to the eye that represent a different power law scaling for volume (thick dashed), D^3, or surface (thick solid), D^2. (c) Polarization asymmetry (blue) and trap aspect ratio (red) obtained from measured spring constants (circles) and from calculations based on the dipole approximation of an oblate spheroid (solid line) and from T-matrix calculations on flat clusters of spheres (dashed lines).

#232608 - $15.00 USD Received 19 Jan 2015; revised 17 Feb 2015; accepted 23 Feb 2015; published 30 Mar 2015

In Fig. 2(a) the force constants divided by the laser power at the trap are shown as a function of the reduced parameter $(\lambda_{trap}-\lambda_p)/\lambda_p$ related to the distance of the trapping wavelength, λ_{trap}, from the in-plane dipole resonance wavelength, λ_p. Solid lines are a fit to the data with a 1/x scaling. As it is clearly observed, trapping constants increase with the red-shifting of the plasmon resonance toward the trapping wavelength. This behaviour is similar to what is observed for Au nanoaggregates [33] and it is related to both the dispersive character of the real part of the polarizability and its increase with particle volume. In Fig. 2(b) the normalized force constants are shown as a function of the nanoplatelets diameter. As expected, trapping constants are higher at increasing particle size. Data are quite comparable to, or even slightly higher than, force constants of spherical particles having the same size, found by both experiments [24,25] and exact electromagnetic calculation of the scattering process [50]. As expected for a Gaussian trapping beam, the spring constant along the beam propagation direction (*z*-axis) is smaller than those obtained in the transverse directions. On the other hand, k_x and k_y are quite comparable. The shape of the trapping potential can be studied by means of two parameters, the polarization asymmetry $k_p = 1 - \frac{k_x}{k_y}$ and the trap aspect ratio $k_{ar} = \frac{k_x + k_y}{2k_z}$, as shown in Fig. 2(c). The first parameter keeps in account the dependence of the spring constants on the trapping beam polarization. The second concerns the anisotropy of the trapping potential.

2.3 Modeling and discussion

To understand the size scaling behaviour observed, we model optical trapping forces using both a dipole approximation and exact electromagnetic calculations based on the use of the Maxwell stress tensor and electromagnetic scattering theory in the T-matrix formalism [51], as shown in Fig. 3. In the first case, we obtain an estimate of the trapping forces by considering our nanoplatelets as oblate spheroids with axis $a_1 = a_2 > a_3$ and using the modified Clausius-Mossotti expression for the particle polarizability [52]. For the case of a cylindrically symmetric Gaussian intensity profile the transverse force constant is obtained from the dipole approximation of the optical force:

$$k_\rho = \frac{2\alpha_d' I_0}{c\varepsilon_0 n_m w_0^2}, \tag{5}$$

where α_d' is the real part of the oblate spheroid polarizability, $I_0 = \frac{2P}{\pi w_0^2}$ is the intensity of the Gaussian beam, w_0 is the beam waist and ε_0 and n_m are the vacuum permittivity and medium (water) refractive index, respectively. The axial spring constant is evaluated by the same expression given above, but considering the Rayleigh range, $z_R = \frac{\pi w_0^2}{\lambda}$, rather than the beam waist. Moreover, to take in account the polarization asymmetry of the focal spot [53], we have used a different size, see also Fig. 3(d)-3(f), for the beam waist in the *x* and *y* direction, so that $w_{0x} \sim 1.5 w_{0y}$, and $w_{0y} = w_0 \sim 0.61\frac{\lambda}{NA}$ estimated by the Abbe criterion for the beam spot size in the diffraction limit, with λ wavelength in the medium. The results are shown in Fig. 2 as solid lines. A good agreement between the measured and dipole approximation values is obtained with no free parameters.

The second approach makes use of electromagnetic scattering theory in the T-matrix formalism [54–57]. The starting point is the calculation of the tightly focused fields by means of the angular spectrum representation [53,58], see Fig. 3(d)-3(f). Thus, optical forces and

#232608 - $15.00 USD Received 19 Jan 2015; revised 17 Feb 2015; accepted 23 Feb 2015; published 30 Mar 2015

torques are calculated in the focal region by means of conservation laws within electromagnetic theory [53]:

$$\mathbf{F}_{\mathrm{Rad}} = r^2 \int_{\Omega} \hat{\mathbf{r}} \cdot \langle \mathsf{T}_{\mathsf{M}} \rangle \, d\Omega \tag{6}$$

$$\Gamma_{\mathrm{Rad}} = -r^3 \int_{\Omega} \hat{\mathbf{r}} \cdot \langle \mathsf{T}_{\mathsf{M}} \rangle \times \hat{\mathbf{r}} \, d\Omega \,, \tag{7}$$

where the integration is over the full solid angle, r is the radius of a large sphere surrounding the particle centre of mass, and $\langle \mathsf{T}_{\mathsf{M}} \rangle$ is the time averaged Maxwell stress in the Minkowski form [51]. The total fields used to calculate this tensor are the superposition of the incident and scattered fields. Both these fields are expanded in a series of vector spherical harmonics, in terms of whose amplitudes cross sections, forces and torques are expressed [41,55]. The multipole amplitudes of the scattered fields are calculated from those of the incident field through the transition matrix [51]. Here the platelets are modeled as planar clusters of coupled spherical sub-units, as shown in Fig. 3(a), whose dimensions are chosen to match the dimensions of the platelets and their optical response, shown in Fig. 3(b). We use the optical constants for silver measured by Johnson & Cristy [59]. In order to ensure the convergence in the multipole expansion, we considered the longitudinal fields and dielectric function, as introduced by Lindhard [60] and simplified by Pack et al. [61]. First, we verified that the equilibrium orientation in the trap is in the *xz* plane by calculating the optical torque along the propagation axis *z*, see Fig. 3(c). Thus, we obtained the force constants for different cluster size shown as dashed lines in Fig. 2(b), 2(c). Also in this case no free parameters have been used and the agreement with experimental data is good. Both dipole approximation and electromagnetic theory catch the size scaling behavior of the data that reflects the planar nature of the plasmonic platelets that follows a surface rather than a volumetric power law.

#232608 - $15.00 USD Received 19 Jan 2015; revised 17 Feb 2015; accepted 23 Feb 2015; published 30 Mar 2015

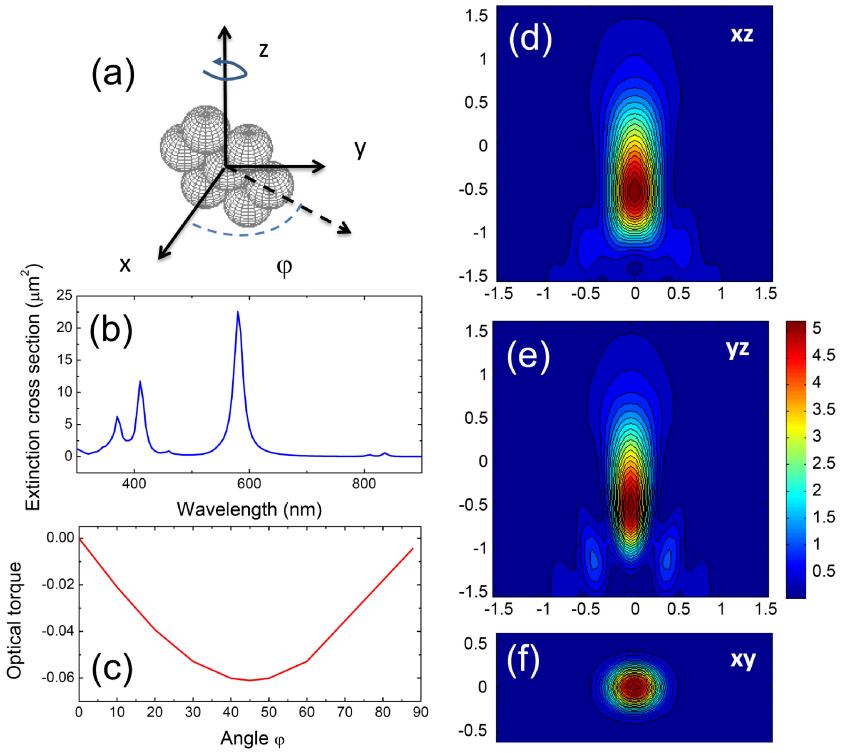

Fig. 3. (a) Cluster model of a silver nanoplatelet. The polarization of the incident field is aligned along *x*, while the propagation axis is along *z*. (b) Extinction cross section for the cluster in (a) showing the different plasmonic bands dictated by the flat geometry. (c) Calculation of the optical torque along *z*, showing that the stable orientation is with the cluster aligned in the *xz* plane ($\varphi = 0$). (d-f) Calculated maps of the field intensity in the focal spot for our experimental parameters ($\lambda_0 = 830$nm, NA = 1.3).

2.4 Surface-enhanced Raman spectroscopy

As a proof of principle, we have used these nanoparticles for SERS applications. A small amount of sample 3 and 4 solutions are drop-cast on a microscope slide. Once dry, an aqueous solution (10^{-4} M) of methylene blue (MB) is deposited on the nanoplatelets. After drying again, micro-Raman spectra (100X obj.) are carried out on a Horiba-Jobin Yvon HR800 Raman spectrometer in back-scattering geometry at 633 nm exciting wavelength. As shown in Fig. 4, a significant increase of Raman signal of MB with respect that obtained on a gold flat substrate, used as a reference [62,63], is observed, with three orders of magnitude SERS amplification.

#232608 - $15.00 USD Received 19 Jan 2015; revised 17 Feb 2015; accepted 23 Feb 2015; published 30 Mar 2015

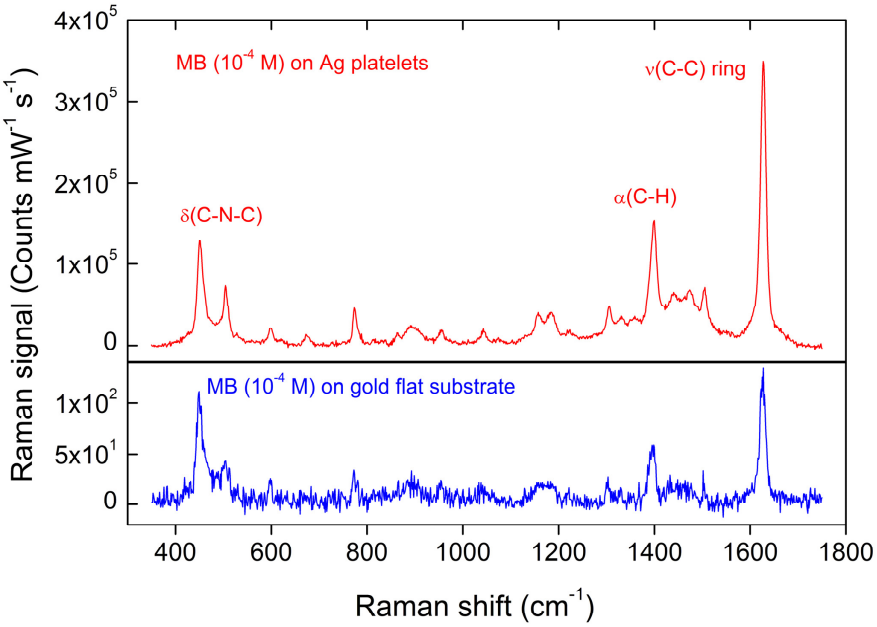

Fig. 4. Raman spectra of a drop-cast 10^{-4} M methylene blue (MB) aqueous solution on a gold flat substrate (blue) and on Ag nanoplatelets (red). The assignment of the most representative peaks [64] is also indicated. A SERS enhancement of three order of magnitude is observed.

3. Conclusions

In this work, we have studied the optical trapping of silver nanoplatelets that can be optically manipulated and used for SERS enhancement of molecular species. These metal nanoparticle samples are produced by a simple and low cost procedure and their plasmonic properties can be tailored in the visible by controlling their diameter. Trapping forces have been measured with force constants normalized to power in the range $10^{-1} \div 10^{-2}$ pN μm^{-1} mW^{-1} that ensures the stable manipulation of these novel structures in water. Furthermore, we modeled the optical trapping on silver nanoplatelets by dipole approximation and by exact electromagnetic scattering calculations within a T-matrix formalism, finding a good agreement. A scaling behavior of optical trapping forces with the square of the particle diameter has been enlightened showing that the two-dimensional shape is the key feature that controls the optomechanical effects on these flat plasmonic systems. Finally, we showed that at least three order of magnitude of SERS enhancement is obtained in the Raman signal of molecules adsorbed on the silver nanoplatelets. The possibility to optical manipulate these colloidal plasmonic nanoparticles and their easy preparation open the way to a widespread use in nano-microscopy and high-resolution molecular spectroscopy in the visible range.

Acknowledgments

We acknowledge support from "Programma Operativo Nazionale Ricerca e Competitività" 2007-2013, project PON01 01322 PANREX, project PAC02L3 00087 SOCIAL-NANO, and the MPNS COST Action 1205 "Advances in Optofluidics: Integration of Optical Control and Photonics with Microfluidics", and MP1302 "Nanospectroscopy".